Projection factor and radii of Type II Cepheids

P. Wielgórski, G. Pietrzyński, W. Gieren, B. Zgirski, M. Górski, J. Storm, N. Nardetto, P. Kervella, G. Bras, G. Hajdu, et al.

A&A, 689, A241 (2024)
https://doi.org/10.1051/0004-6361/202450182

Astronomy & Astrophysics

Projection factor and radii of Type II Cepheids

BL Her stars

P. Wielgórski[1,⋆], G. Pietrzyński[1,2], W. Gieren[2], B. Zgirski[2], M. Górski[1], J. Storm[3], N. Nardetto[4], P. Kervella[5], G. Bras[5], G. Hajdu[1], V. Hocdé[1], B. Pilecki[1], W. Narloch[1], P. Karczmarek[2], W. Pych[1], R. Chini[1,6,7], and K. Hodapp[8]

[1] Nicolaus Copernicus Astronomical Center, Polish Academy of Sciences, Bartycka 18, 00-716 Warszawa, Poland
[2] Universidad de Concepción, Departamento de Astronomia, Casilla 160-C, Concepción, Chile
[3] Leibniz-Institut für Astrophysik Potsdam (AIP), An der Sternwarte 16, 14482 Potsdam, Germany
[4] Université Côte d'Azur, Observatoire de la Côte d'Azur, CNRS, Laboratoire Lagrange, France
[5] LESIA, Observatoire de Paris, Université PSL, CNRS, Sorbonne Université, Université Paris Cité, 5 place Jules Janssen, 92195 Meudon, France
[6] Astronomisches Institut, Ruhr-Universität Bochum, Universitätsstrasse 150, 44801 Bochum, Germany
[7] Instituto de Astronomía, Universidad Católica del Norte, Avenida Angamos 0610, Antofagasta, Chile
[8] University of Hawaii, Institute for Astronomy, 640 N. Aohoku Place, Hilo, HI 96720, USA

Received 29 March 2024 / Accepted 1 June 2024

ABSTRACT

Context. Type II Cepheids are old pulsating stars that can be used to trace the distribution of an old stellar population and to measure distances to globular clusters and galaxies within several megaparsecs, and by extension, they can improve our understanding of the cosmic distance scale. One method that can be used to measure the distances of Type II Cepheids relies on period-luminosity relations, which are quite widely explored in the literature. The semi-geometrical Baade-Wesselink technique is another method that allows distances of radially pulsating stars, such as Type II Cepheids, to be measured if the so-called projection factor is known. However, the literature concerning this parameter for Type II Cepheids is limited to just a few pioneering works.
Aims. In determining projection factors for eight nearby short-period Type II Cepheids, also known as BL Her type stars, we aim to calibrate the Baade-Wesselink method for measuring distances for this class of stars.
Methods. Using the surface brightness-colour relation version of the Baade-Wesselink technique, we determined the projection factors and radii of eight nearby BL Her type stars. We adopted accurate distances of target stars from *Gaia* Data Release 3. Time series photometry in the V and K_S bands have been collected with two telescopes located at the *Rolf Chini* Cerro Murphy Observatory (former Cerro Armazones Observatory), while spectroscopic data have been obtained within dedicated programmes with instruments hosted by the European Southern Observatory.
Results. The measured projection factors for the stars with good quality data are in the range between 1.21 and 1.36. The typical uncertainty of projection factors is 0.1. The mean value is 1.330 ± 0.058, which gives the uncertainty of ~4%. The main sources of uncertainty on the p-factors are statistical errors of the Baade-Wesselink fit (related to the dispersion and coverage of light and radial velocity curves) and parallax. In the case of radii, the biggest contribution to the error budget comes from the K_S band photometry's systematic uncertainty and parallax. The determined radii allowed us to construct the period-radius relation for BL Her stars. Our period-radius relation is in good agreement with the previous empirical calibration, while two theoretical calibrations found in the literature agree with our relation within 2σ. We also confirm that BL Her and RR Lyr stars obey an apparent common period-radius relation.

Key words. stars: distances – stars: Population II – stars: variables: Cepheids

1. Introduction

Radially pulsating stars, such as Cepheids (classical, Type II, or anomalous) and RR Lyrae, serve as very important distance indicators. What makes them very special is that there are two completely independent methods of determining distances to these stars that take advantage of their pulsational nature. The respective period-luminosity relations of pulsating stars (Leavitt Law; Leavitt 1908) make them widely usable as very precise standard candles (e.g. Gieren et al. 2005; Ripepi et al. 2017; Riess et al. 2021; Beaton et al. 2016; Bhardwaj 2020; Breuval et al. 2023; Sicignano et al. 2024). In particular, the period-luminosity relation for classical Cepheids is used in the most precise distance ladder to determine the *Hubble Constant* (Riess et al. 2023). On the other hand, the semi-geometric Baade-Wesselink (BW) method (it is also sometimes called the Baade-Becker-Wesselink or parallax-of-pulsation method; Baade 1926; Becker & Strohmeier 1940; Wesselink 1947) can be applied to measure the distance to the radially pulsating star by comparing variations of the physical (inferred from integration of the radial velocity curve) and apparent angular size (obtained from photometry or interferometry). Different versions of the BW method have been applied by many authors to obtain distances and sizes of pulsating stars (e.g. Balona 1977; Burki & Meylan 1986; Gieren et al. 1998; Rastorguev & Dambis 2011; Groenewegen 2013; Ripepi et al.

⋆ Corresponding author; pwielgor@camk.edu.pl

2014; Mérand et al. 2015). This method requires prior knowledge of the so-called projection factor (p-factor), which translates the radial velocity measured from spectra into the velocity of the expanding or contracting atmosphere of the star (pulsational velocity). The value of the p-factor is the result of the projection of the pulsational velocity from a given part of the visible stellar disc on the line of sight. Due to limb darkening, velocity gradients in the atmosphere, and other factors, the value of the p-factor is difficult to model (see, e.g., Nardetto et al. 2011, 2014, and references therein). An accurate calibration of this parameter is crucial to achieve high accuracy on distances measured with the BW method.

Empirical determination of the projection factor requires prior knowledge of the distances of a sample of stars of a given class. While parallaxes of a number of classical Cepheids and RR Lyrae stars were measured by HIPPARCOS and the *Hubble* Space Telescope, the Type II Cepheid distance scale was based on parallaxes of just two stars before *Gaia* (Matsunaga et al. 2009; Benedict et al. 2011). The *Gaia* space mission (Gaia Collaboration 2016) is a game-changer, and the last data release (Data Release 3, DR3, Gaia Collaboration 2021; Lindegren et al. 2021b) contains parallaxes of several dozens of Type II Cepheids within 5 kpc. In Wielgórski et al. (2022), we used *Gaia* DR3 parallaxes of 21 Galactic Type II Cepheids to determine period-luminosity relations with an accuracy of ∼5%.

Different versions of the BW analysis have been used to determine radii of Type II Cepheids assuming the value of the p-factor (e.g. 1.36, Balona 1977; Burki & Meylan 1986; Balog et al. 1997). The literature concerning p-factors of Type II Cepheids is limited to just some pioneering works (Feast et al. 2008; Breitfelder et al. 2015; Pilecki et al. 2018). Two stars analysed in these papers are peculiar W Virginis (pW Vir) stars, which are believed to be members of binary systems, which is a quite strong limitation for using them as precise distance indicators. Feast et al. (2008) used the HIPPARCOS parallax of κ Pav in an analysis that is similar to what is presented in this paper and obtained a very low p-factor value of 0.93 ± 0.11. Breitfelder et al. (2015) analysed κ Pav with the Spectro-Photo-Interferometry of Pulsating Stars code (`SPIPS`) Mérand et al. 2015), which utilises multiband photometric and interferometric datasets and models of stellar atmospheres to determine the angular size of the star, and they obtained $p = 1.26 \pm 0.07$. We note that κ Pav is believed to belong to the pW Vir class (Matsunaga et al. 2009; Wielgórski et al. 2022); however, no signature of a companion has been found so far. On the other hand, Pilecki et al. (2018) performed a very detailed analysis of pW Vir found by the Optical Gravitational Lensing Experiment (*OGLE*, Udalski et al. 2008; Soszyński et al. 2008) project in the Large Magellanic Cloud, which is a known eclipsing binary. The value of the projection factor obtained in that study is 1.30 ± 0.03.

Recent studies of p-factors for classical Cepheids (Trahin et al. 2021) and RR Lyrae stars (Bras et al. 2024) with `SPIPS` and using accurate parallaxes from the *Gaia* satellite mission have revealed quite a big scatter (∼10%) and no clear correlation of p-factors with the period. On the other hand, Gallenne et al. (2017) in their analysis of classical Cepheids in the Large Magellanic Cloud with `SPIPS` obtained a quite significant linear dependence of the p-factor on the period. The observed large scatter (not compatible with the statistical errors of the measured p-factors) of p-factors could be the result of the non-uniform datasets used in the analysis (different instruments and epochs of observations); cycle-to-cycle variations of the radial velocity amplitude (Anderson et al. 2016; Anderson 2016); the gradient of the velocity in the stellar atmosphere (Nardetto et al. 2017); or even envelopes composed of dust or ionised gas surrounding these stars (Kervella et al. 2009; Hocdé et al. 2020; Nardetto et al. 2023; Hocdé et al. 2024). This may also suggest that using a single parameter to translate the observed radial velocity into the pulsational velocity of the stellar atmosphere is too great of a simplification, but we believe that there is still some space for improvements both in the data and methodology. Comparing projection factors for different types of pulsating stars with different physical properties can also be very helpful in improving our understanding of stellar atmospheres.

In this study, we present the very first determination of the p-factor for Type II Cepheids of the BL Her subclass using the surface brightness-colour relation (SBCR) version of the BW method (Barnes & Evans 1976; Fouque & Gieren 1997). Our sample consists of eight stars, but it will be expanded in the future, which should allow us to check the intrinsic scatter of the p-factor and its dependence on other parameters. This work is part of a series of papers on the Araucaria project (The Araucaria Project 2023) devoted to the calibration of primary distance indicators using nearby stars and is based on observations made at the *Rolf Chini* Cerro Murphy Observatory (OCM; formerly the Cerro Armazones Observatory; Ramolla et al. 2016) and *Gaia* parallaxes. Thanks to the use of uniform datasets, as described in Section 2, we minimised the influence of systematic errors on our results. In Section 3, we present our methodology, and Section 4 presents our results and discussion. We summarise our work in Section 5.

2. Data

2.1. Optical and near-infrared photometry, reddening, and periods

The photometric data were collected between March 2017 and March 2020 with two telescopes located at OCM. Near-infrared time series data in the J, H, and K_S passbands, collected with the IRIS camera (Hodapp et al. 2010) installed on the 0.8-metre telescope, have been published in Wielgórski et al. (2022). In this work, we used the K_S band data only. We supplemented our K_S band measurements for SW Tau with data from Feast et al. (2008), collected with a photometer installed on the 0.75-metre telescope at the South African Astronomical Observatory (SAAO). The IRIS photometry is in the Two Micron All Sky Survey (2MASS, Skrutskie et al. 2006) system, and we transformed the SAAO photometry to the 2MASS system using formulae from Koen et al. (2007). The systematic uncertainty of the K_S band light curves was estimated in Wielgórski et al. (2022) to 0.02mag.

Optical photometry in the Johnson B and V passbands were obtained with the *VYSOS*16 0.4-metre telescope located at OCM (Ramolla et al. 2013) with a pixel scale of 0.77 arcsec/px and a $41.2' \times 25.5'$ field of view. Nine dithered images were corrected for dark current and flatfielded with the standard `IRAF` routines (Tody 1993) and then matched and stacked into one final frame using `Sextractor` (Bertin & Arnouts 1996); `SCAMP` (Bertin 2006); and `SWARP` (Bertin 2010). Aperture photometry was made with a dedicated pipeline based on the `Astropy` Python library (Astropy Collaboration 2018), and `DAOPHOT` (Stetson 1987) was transformed to the standard Johnson-Cousins system using secondary standards from the synthetic all sky catalogue described in Gaia Collaboration (2023), which was created based on *Gaia* low-resolution spectra. The synthetic

catalogue was standardised with Landolt (1992) standard fields, and the authors estimated its accuracy with secondary standards from the 'Stetson collection' (for details see section 3.2 in Gaia Collaboration 2023) to be at the level of ∼0.02 mag. We adopted this value as the systematic uncertainty of our transformations. We selected as secondary standards three to ten stars with a brightness comparable to the target star and a wide range of colours. The $(B-V)$ colour term of our transformations to the standard system is −0.04 for the B band and zero for the V band. The B and V band photometric data are presented in Table 1.

We adopted periods published in Wielgórski et al. (2022) and presented in Table 2. In the case of SW Tau, the period given in the table is for $HJD = 2435500.0$, and we applied the period change of -1.15×10^{-6} s/yr from Devlen & Acar (2017) to improve the quality of curves, in particular to phase the K_S band measurements from IRIS and Feast et al. (2008) and by extension to minimise the spread of the final fit.

Our light curves are quite well sampled, but in some cases we decided to fit templates to our measurements in the V band. Templates were created using photometry of a given star in the V band from the All Sky Automated Survey (ASAS; Pojmański 2004) or from the All Sky Automated Survey for Supernovae (ASASSN; Shappee et al. 2014; Jayasinghe et al. 2018), depending on the quality of the photometry from a given source. The ASAS or ASASSN photometry was phased with a period given in Table 2 and approximated with Akima splines (Akima 1970), implemented in the `SciPy` Python library (Virtanen et al. 2020). The template light curve was then fit (amplitude, phase shift, and mean magnitude) to our measurements using χ^2 minimisation. In Figure 1, we show the exemplary photometry used to create the template.

The photometry was corrected for the interstellar extinction using values of the colour excess $E(B-V)$ published in Wielgórski et al. (2022), which are based on Schlafly & Finkbeiner (2011) reddening maps and the dust model in the Milky Way from Drimmel & Spergel (2001). To calculate the total extinction in V and K_S bands, we used Cardelli et al. (1989) and O'Donnell (1994) reddening law, assuming $R_V = 3.1$. The adopted values of $E(B-V)$ are also presented in Table 2. The statistical uncertainty given in Schlafly & Finkbeiner (2011) is below 0.01 mag, but we assumed the uncertainty of the $E(B-V)$ values to be at the level of 0.02 mag.

Table 1. New optical photometry of the Type II Cepheid sample analysed in this paper.

Star	Filter	HJD (days)	m (mag)	σ_m (mag)
BL Her	V	2458342.531808	9.792	0.005
BL Her	V	2458344.533328	10.386	0.005
BL Her	V	2458346.538110	9.894	0.005
BL Her	V	2458347.533630	10.441	0.005
BL Her	V	2458348.547888	10.470	0.005
BL Her	V	2458349.540027	10.226	0.005
BL Her	V	2458350.536321	9.963	0.005
BL Her	V	2458351.534698	10.227	0.005
BL Her	V	2458352.530724	10.548	0.005
BL Her	V	2458353.525130	10.319	0.005
BL Her	V	2458355.525918	9.837	0.005
BL Her	V	2458356.519569	10.601	0.005
BL Her	V	2458357.494819	10.330	0.005
BL Her	V	2458358.495066	10.001	0.005
BL Her	V	2458359.495035	9.770	0.005
BL Her	V	2458368.551779	10.090	0.005
BL Her	B	2458342.525882	10.045	0.009
BL Her	B	2458344.527333	10.929	0.006
BL Her	B	2458346.532184	10.188	0.006
BL Her	B	2458347.527763	10.979	0.005
BL Her	B	2458348.531766	11.041	0.005

Notes. The full version of this table is available as supplementary material in a machine readable format at the CDS.

2.2. Spectroscopy

Radial velocities were measured from spectra collected between 2016 and 2023 within dedicated programmes with four high resolution (40 000–100 000) spectrographs hosted by the European Southern Observatory (ESO). We used CORALIE, installed on the 1.2m 'Swiss' Leonhard Euler telescope at La Silla Observatory (Queloz et al. 2000); HARPS, installed on the 3.6m telescope at La Silla Observatory (Pepe et al. 2000); FEROS, installed on the 2.2m MPG/ESO telescope at La Silla Observatory (Kaufer & Pasquini 1998); and UVES, installed on the 8.2m VLT UT2 (Kueyen) telescope at the Paranal Observatory (D'Odorico et al. 2000, filler programme).

In the case of HARPS and UVES spectra, we used the standard reduction pipelines (instrumental calibrations and wavelength solution) offered by ESO and downloaded processed spectra from the ESO archive. The CORALIE and FEROS spectra were reduced with `CERES` pipeline (Brahm et al. 2017), which proved to give good results for these two instruments. If needed, we merged the echelle orders with a custom Python script developed by our team and normalised spectra by modelling continuum with polynomials (after excluding the most prominent lines). As shown by Nardetto et al. (2008) and Borgniet et al. (2019), the selection of the analysed spectral lines has an impact on the obtained value of the p-factor. To homogenise the spectra from all instruments, we restricted the analysis to the wavelength range between 450 nm and 650 nm. Moreover, we used a mask to exclude telluric lines and problematic regions (such as gaps) present in some spectra.

Radial velocities were measured using the cross-correlation function (CCF) implemented in `iSpec` software (Blanco-Cuaresma et al. 2014) using Coelho et al. (2005) synthetic spectra as templates. We also tried the Broadening Function (BF) technique implemented in `Ravespan` (Pilecki et al. 2017), but it gave virtually identical results. The important concern that quite significantly impacts the obtained results is the selection of the function to model the CCF, as the profiles of lines for pulsating stars are asymmetric in some phases. We decided to use the Gaussian profile to be consistent with Trahin et al. (2021) and Bras et al. (2024), but we also tried a bi-Gaussian profile and first moment as described in Nardetto et al. (2017), and we discuss the influence of this choice on the results. The typical uncertainty of our radial velocity measurements is 0.2 km/s. We did not observe any obvious systematic shift between the measurements from different instruments. The measured radial velocities are presented in Table 3.

2.3. Distances

Similar to Wielgórski et al. (2022), we used parallaxes from *Gaia* DR3 with the position, magnitude, and colour-dependent zero-point offset calculated with the dedicated Python code

Table 2. Periods, parallaxes, parallax zero-point offset, *Gaia* G-band magnitude and $(Bp - Rp)$ colour index, and reddening for the analysed Type II Cepheids.

Name	P (days)	ω (mas)	ZPO (mas)	G_{Gaia} (mag)	$(Bp - Rp)$ (mag)	$E(B - V)$ (mag)
(1)	(2)	(3)	(4)	(5)	(6)	(7)
VY Pyx	1.239957	3.9495 ± 0.0186	−0.0237	7.11	0.81	0.048 ± 0.02
BL Her	1.30743	0.8469 ± 0.0179	0.0016	10.17	0.74	0.067 ± 0.02
KZ Cen	1.52006	0.3024 ± 0.0153	−0.0224	12.37	0.74	0.084 ± 0.02
SW Tau	1.58355*	1.2244 ± 0.0222	−0.0103	9.62	0.98	0.252 ± 0.02
V971 Aql	1.62453	0.4400 ± 0.0219	−0.0175	11.78	0.91	0.174 ± 0.02
V439 Oph	1.89298	0.4753 ± 0.0163	−0.0103	11.89	1.15	0.268 ± 0.02
RT TrA	1.94612	1.0162 ± 0.0162	−0.0021	9.68	0.92	0.112 ± 0.02
FM Del	3.95498	0.2300 ± 0.0135	−0.0174	12.27	0.92	0.087 ± 0.02

Notes. Period for $HJD = 2435500.0$, period change -1.15×10^{-6} s/yr

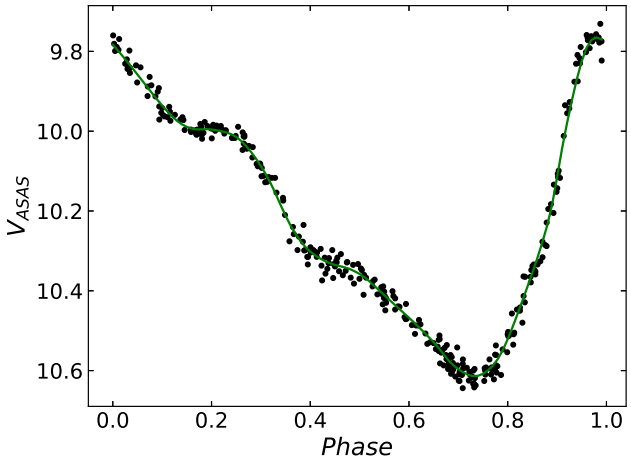

Fig. 1. *ASAS* photometry used to create the V band light curve template for BL Her star. The green line is the Akima spline fit.

described in Lindegren et al. (2021a). We increased the statistical uncertainties of the parallaxes given in the *Gaia* catalogue by 10% as suggested by Riess et al. (2021) to account for possible excess uncertainty. The values of the parallaxes and zero-point corrections as well as the *Gaia* G-band magnitudes and $(Bp - Rp)$ colour index used to calculate the zero-point corrections are given in Table 2.

The renormalised unit weight error (RUWE) and goodness of fit (GOF) parallax quality parameters given in the *Gaia* catalogue (see Table 2 in Wielgórski et al. 2022) for the analysed stars are well below the limits for good quality parallaxes ($RUWE < 1.4$, $GOF < 12.5$, Lindegren et al. 2021b). The distances of the stars in our sample are between 250 pc and 4500 pc, with a mean value of 900 pc and typical error of ∼2%.

3. The IRSB Baade-Wesselink method

Our implementation of the BW method is similar to the approach presented in Storm et al. (2011) and Gieren et al. (2018). It relies on the angular diameters determined from the SBCR (Barnes & Evans 1976) calibrated for the $(V - K_s)$ colour index (IRSB technique, Fouque & Gieren 1997). The angular diameters determined this way very weakly depend on reddening, metallicity, or surface gravity (Fouque & Gieren 1997; Kervella et al. 2004a; Gieren et al. 2018; Pietrzyński et al. 2019; Thompson et al. 2001; Salsi et al. 2022). The surface brightness F_V is defined as follows:

$$F_V(\phi) = 4.2207 - 0.1V_0(\phi) - 0.5 \log \theta(\phi), \quad (1)$$

where V_0 is the unreddened V band magnitude and θ is the angular diameter. Calibrations of the SBCR have been made for different types of stars by, for example, Welch (1994), Fouque & Gieren (1997), di Benedetto (1998), Kervella et al. (2004b,a), Challouf et al. (2014), Pietrzyński et al. (2019), Graczyk et al. (2021), Salsi et al. (2021) from interferometric measurements of angular diameters or eclipsing binaries with known distances. There is no specific relation calibrated for Type II Cepheids (which are giants of F-G spectral type) available, so we decided to use the relations from Kervella et al. (2004a, hereafter K04a); Kervella et al. (2004b, K04b); Salsi et al. (2021, S21); and Graczyk et al. (2021, G21), which are presented in Table 4. We decided to use these relations because they are independent and very precise (dispersion ∼1–2%) and cover the colour range of the analysed Type II Cepheids. These relations are calibrated for classical Cepheids, dwarfs, and subgiants, and such an approach allowed us to test the influence of the uncertainty of the surface brightness on the obtained results. The relations are also presented in Figure 2 together with the colour index range covered by each star during the pulsation cycle.

The light and radial velocity curves were phased with HJD_0 set to the maximum of brightness in the V band. We then fit the Akima spline polynomials (Akima 1970), implemented in the `SciPy` Python library (Virtanen et al. 2020) or template (created from ASAS or ASASSN data), to the V band light curve and radial velocity curve. We found the mean radial velocity V_γ by integrating the radial velocity curve, and then we calculated the following integral:

$$\Delta R'(\phi_i) = \frac{\Delta R(\phi_i)}{p} = \int_0^{\phi_i} -(V_r(\phi) - V_\gamma) P \mathrm{d}\phi, \quad (2)$$

which gave us the displacement (in kilometres) of the physical radius $\Delta R(\phi_i)$ over the pulsation phase but divided by the projection factor p. We found the mean value of $\Delta R'(\phi_i)$ and subtracted it from the above integral to obtain the displacement relative to the mean radius of the star.

From the model of the V band light curve, K_S band measurements, and the reddening correction, we obtained the unreddened $(V - K_S)_0$ colour index for the phases corresponding to the phases of the K_S band measurements. From the selected SBCR,

Table 3. New radial velocity measurements of the sample Type II Cepheids analysed in this paper.

Star	HJD (days)	$V_{r,G}$ (km/s)	σ_{V_r} (km/s)	$V_{r,C}$ (km/s)	$V_{r,B}$ (km/s)	Instrument
BL Her	2457901.69869132	18.11	0.20	25.95	18.17	HARPS
BL Her	2457901.77199208	−2.07	0.13	−0.98	−2.10	HARPS
BL Her	2457902.68274749	20.32	0.07	18.17	20.36	HARPS
BL Her	2457903.75918934	10.23	0.08	12.32	10.19	HARPS
BL Her	2457914.67843204	36.17	0.13	32.12	36.22	HARPS
BL Her	2457914.76888472	20.27	0.32	26.88	20.27	HARPS
BL Her	2457915.62648906	12.07	0.06	12.01	12.09	HARPS
BL Her	2457915.72868948	18.09	0.06	16.44	18.14	HARPS
BL Her	2457916.67453464	8.31	0.06	8.24	8.29	HARPS
BL Her	2458233.77712936	26.60	0.28	29.33	26.59	HARPS
BL Her	2458240.78722272	3.05	0.05	−1.86	3.11	CORALIE
BL Her	2458240.8691601	6.04	0.05	4.90	6.02	CORALIE
BL Her	2458240.92456825	8.57	0.04	7.41	8.58	CORALIE
BL Her	2458241.78463846	−10.76	0.16	−8.45	−10.81	CORALIE
BL Her	2458241.86983985	−8.34	0.13	−8.51	−8.30	CORALIE
BL Her	2458242.82536589	36.15	0.07	32.66	36.17	CORALIE
BL Her	2458243.87606979	16.88	0.05	17.38	16.92	CORALIE

Notes. Measurements were obtained from a cross-correlation function modelled with Gaussian ($V_{r,G}$), centroid ($V_{r,C}$), and bi-Gaussian ($V_{r,B}$). The full version of this table is available as supplementary material in a machine readable format at the CDS.

Table 4. Surface brightness-colour relations used to estimate the angular diameters of Type II Cepheids.

Abbreviation	Relation	Calibrating sample	Source
K04a	$F_V = -0.1336 \times (V-K)_0 + 3.9530$	classical Cepheids $0.95 < (V-K_S)_0 < 2.4$	Kervella et al. (2004a)
K04b	$F_V = -0.1377 \times (V-K)_0 + 3.9620$	dwarfs and subgiants $0.5 < (V-K_S)_0 < 3$	Kervella et al. (2004b)
S21	$F_V = -0.1404 \times (V-K)_0 + 3.9665$	dwarfs and subgiants $1 < (V-K_S)_0 < 3$	Salsi et al. (2021)
G21	$F_V = -0.0031 \times (V-K)_0^5 + 0.0239 \times (V-K)_0^4$ $-0.0623 \times (V-K)_0^3 + 0.0705 \times (V-K)_0^2$ $-0.1708 \times (V-K)_0 + 3.9666$	dwarfs $0.5 < (V-K_S)_0 < 2.1$	Graczyk et al. (2021)

we then calculated the surface brightness F_V for a given phase of K_S band measurements, and then from equation (1), we calculated the angular size θ (in miliarcseconds) of the star in a given phase. Relations from Salsi et al. (2021) and Graczyk et al. (2021) are given for K_s photometry in the $2MASS$ system, but in the case of Kervella et al. (2004a,b), which are in the $SAAO$ system, we transformed our K_S band photometry using equations from Koen et al. (2007).

The angular size for a given phase $\theta(\phi)$ and the physical radius $R(\phi)$ are connected by the following geometrical formula:

$$\theta(\phi_i) = 6.7114 \times 10^{-9} \times 2\omega R(\phi_i), \tag{3}$$

where ω is the parallax (in milliarcseconds) and the numerical constant comes from changing parsec to kilometres and radians to milliarcseconds (it is in fact simply the inverse of the astronomical unit). Using equation (2), we obtained the following relation:

$$\theta(\phi_i) = 6.7114 \times 10^{-9} \times 2\omega(p\Delta R'(\phi_i) + \langle R \rangle), \tag{4}$$

where $\langle R \rangle$ is the mean radius of the star. By fitting a straight line to this relation, we obtained the projection factor (as a slope) and the mean angular diameter of the star (the zero point), which is used to calculate the mean radius.

4. Results and discussion

Figure 3 and Figures A.1–A.7 in Appendix A present the light and radial velocity curves (panels *a*,*b*,*d*), the $(V - K_S)$ colour index curve (panel *c*), the integrated radial velocity (panel *e*), and the angular diameter curve based on K04b SBCR (panel f) for the analysed stars. Panel *g* shows the linear relation between the angular diameter and the integrated radial velocity in corresponding phases rescaled using equation (4) to have identical units in both axes. The slope of the fitted line is simply the *p*-factor in such a case, and the zero point is the mean angular size of the star, which is used to calculate the mean radius. In panel *f*, we also plot the integrated radial velocity curve from panel *e*, rescaled using equation (4), and the estimated values of the *p*-factor and mean radius. In the cases of VY Pyx, SW Tau, V971 Aql, and V439 Oph, the V band light curve was approximated with Akima splines, while for BL Her, KZ Cen, RT TrA, and FM Del, we used a template created based on the ASAS or ASASSN V band light curve of a given star.

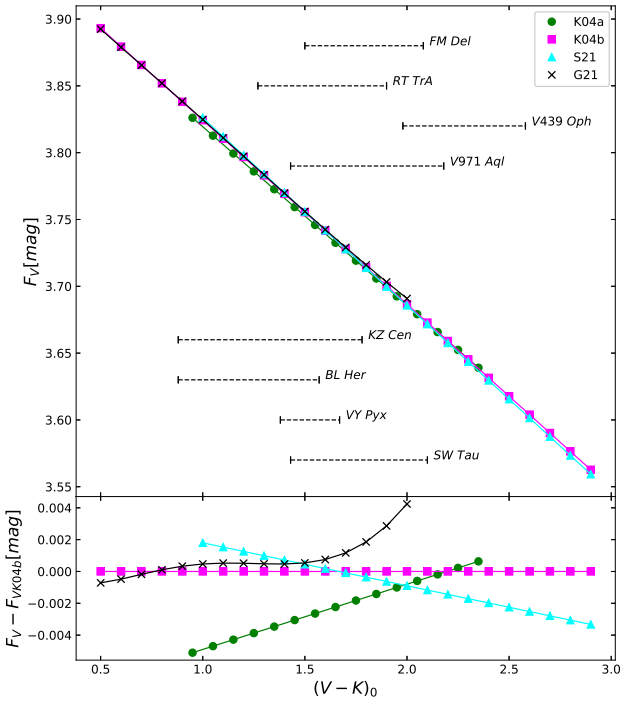

Fig. 2. Surface brightness-colour relation used to determine the angular diameters of the analysed stars. The dashed sections denote the colour index range covered by each analysed star during the pulsation cycle.

Statistical uncertainties on the obtained values of the p-factors and radii were evaluated in the Monte-Carlo process. In each simulation, we drew V and K_S band and radial velocity measurements from normal distributions defined by the original measurements and related errors and perform the BW analysis. We repeated this process 2000 times, and from the resulting histograms of the p-factor and radius, we obtained the uncertainties as the standard deviation of a Gaussian fitted to the histogram. In Figure 4, we show the scatter plot for the p-factor and mean radius obtained in Monte-Carlo simulations for V439 Oph and respective histograms for these two parameters. The Pearson correlation coefficient r for the p-factor and mean radius for each analysed star is between −0.2 and 0.2, which means that the correlation between these two parameters is very weak.

The obtained values of the p-factors and radii obtained using different SBCRs with statistical errors resulting from the Monte-Carlo simulations are summarised in Table 5. As the relation K04b covers the whole range of the colours of all analysed Type II Cepheids and gives in most cases the smallest dispersion of the final fit, we used it as a reference relation. We used the other SBCRs to estimate the uncertainty related to the uncertainty of the surface brightness. In Figure 5, we show for comparison the relation from panel g of Figure 3 for the star V439 Oph but for each SBCR used in the analysis.

We tested the influence of the systematic errors of the V and K_S band photometry, $E(B-V)$, and parallax on our results. We simply shifted a given curve or parameter by the assumed systematic value (0.02 mag for V and K_S light curves, and errors from Table 2 for reddening and parallax), and we repeated the whole process to find the corresponding value of the p-factor and radius. The difference between the value obtained with the original dataset and the value obtained after applying the systematic shift gave us the uncertainty related to the uncertainty of a given parameter.

The spread of the obtained values of the p-factors and radii from different SBCRs was adopted as the uncertainty related to the surface brightness. The obtained uncertainties for every star are summarised in Table 6. The total errors on the p-factors and radii are the quadratic sum of the uncertainties detailed in this Table for each star.

We note that SW Tau is the only star for which we used the K_S band photometry from two sources, and we had to apply the period change to phase the curves. In Figure 6, we plot the relation from panel f of Figure A.4, but the measurements based on different K_S band photometry sources are marked with different colours. The p-factor obtained based only on IRIS data amounts to 1.26 ± 0.11, while using photometry from Feast et al. (2008) gives a value of 1.32 ± 0.04. Both values are in agreement within the statistical error with the value obtained using the combined IRIS and Feast et al. (2008) data, which amounts to 1.32 ± 0.04. In the case of radii, we obtained 9.29 ± 0.03 and 9.15 ± 0.01 when we exclusively used IRIS and Feast et al. (2008), respectively. These values differ by ∼1.6%, which is most probably caused by a small systematic difference (0.015 mag) in the K_S light curves of these two sources.

4.1. Projection factors

The values of the p-factor for the reference K04b relation mostly range between 1.21 and 1.36, and the results for different SBCRs are usually in agreement within statistical errors. One significantly outlying star, VY Pyx, is the brightest star in our sample (brighter than 6 mag in K_S) and has a very low amplitude (0.3 mag in V and K_S). It was observed with the non-cooled neutral density filter, which increased the thermal noise and results with a low-quality K_S band light curve. These factors result in the low precision of the fit. The weighted mean value of the p-factors, including VY Pyx, is 1.330 ± 0.058, and the standard deviation amounts to 0.143. When we excluded VY Pyx, we obtained a weighted mean of 1.314 ± 0.022 and a standard deviation of 0.054. These mean values of the p-factor are in good agreement (1σ) with the values obtained for peculiar W Vir stars in Breitfelder et al. (2015) and Pilecki et al. (2017), which are 1.26 ± 0.07 and 1.30 ± 0.03, respectively.

From Table 6, one can see that the most significant sources of errors on p-factors in most cases are the statistical spread of the final BW fit, which is connected to the dispersion and coverage of light and radial velocity curves and can be minimised with a higher number of measurements, and parallax, which will be also improved in the future with the final *Gaia* data release. As expected, the influence of reddening on the obtained results is negligible (below 1%). The systematic shift of the V band light curve gives a change of p-factor below 1%, and for K_S, it is at the level of 1.5%. Errors related to the uncertainty of the surface brightness are at the level of 2–3%.

In Figure 7, we plot the relation between the p-factors and the logarithms of periods of the analysed stars. The errors of the p-factors are the total errors from Table 6 (every source of the error in this table contributes to the observed dispersion of the p-factors in this plot), and in most cases the measured values of the p-factors are in agreement with the mean value within 1σ. No obvious relation between the p-factor and the period is visible, so at this stage we can conclude that for short-period Type II Cepheids, it is sufficient to use the constant value of the p-factor given above.

Recently, Zgirski et al. (2024) used the same method and data from identical instruments as in this work to measure the p-factors of nine RR Lyr stars. They obtained a mean value of

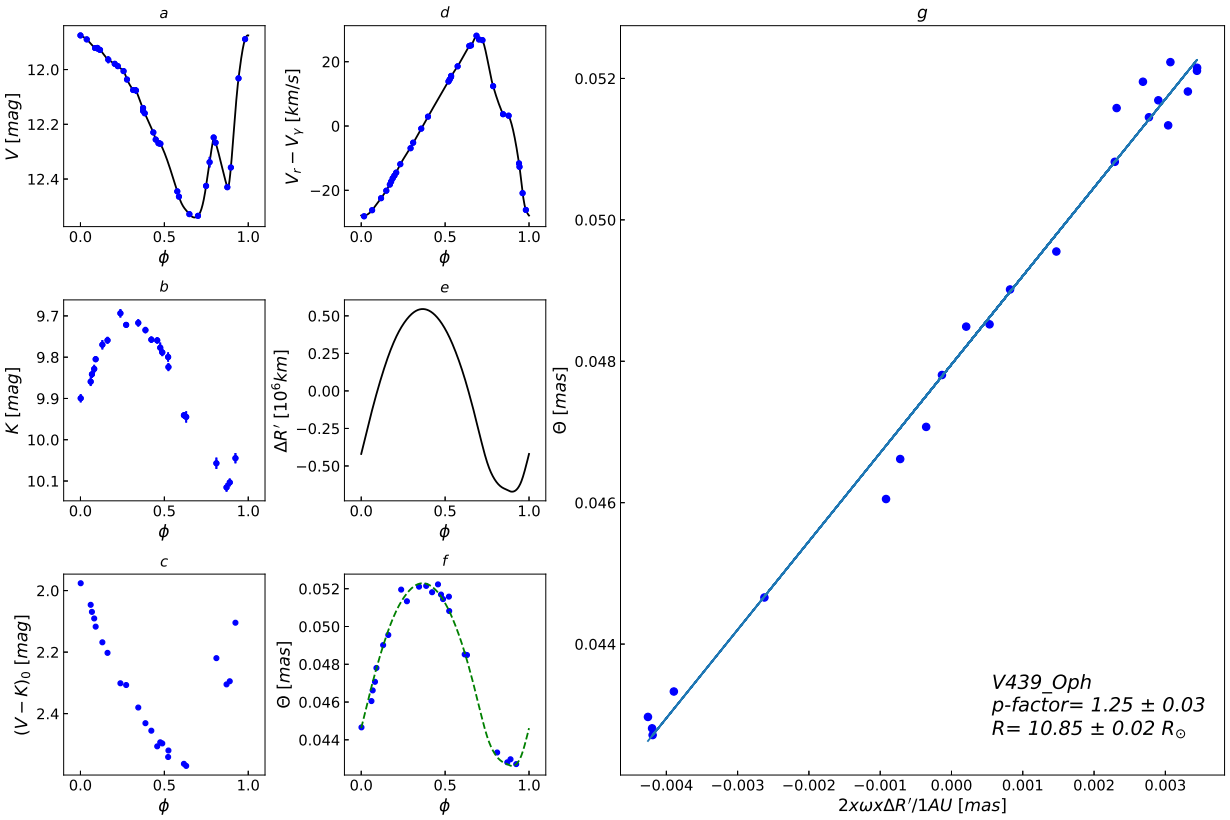

Fig. 3. Baade-Wesselink analysis of V439 Oph. Panels *a*, *b*, and *d* show our V, K_S, and radial velocity measurements, respectively. Panel *c* shows the unreddened colour index curve. Black lines in these plots are Akima splines fitted to the measurements. Panel *e* shows the integrated radial velocity curve. Panel *f* shows the angular diameter measured using the K04b SBCR. The green line in this panel is the curve from panel *e*, rescaled using equation 4 and measured values of the *p*-factor and the mean radius. Panel *g* shows the relation between angular diameters from panel *f* and corresponding values of the integrated radial velocity from panel *e*, rescaled using equation (4). The slope of this relation is the *p*-factor, and the zero point is the mean angular diameter used to calculate the mean radius of the star.

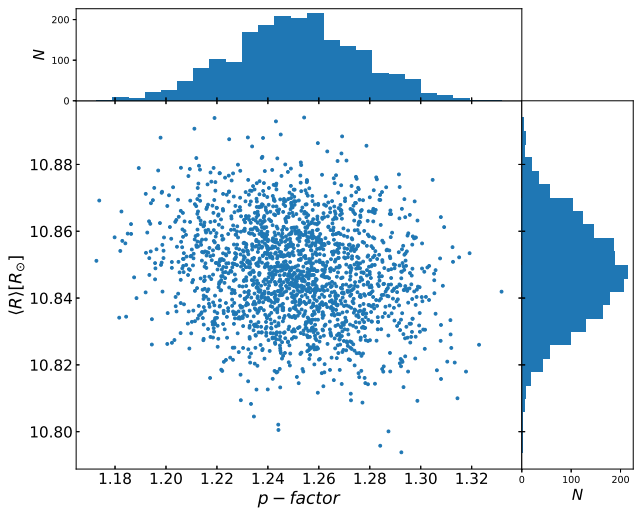

Fig. 4. Scatter plot for the *p*-factor and mean radius from 2000 Monte-Carlo simulations and respective histograms for both parameters for V439 Oph.

1.44 ± 0.03, which is higher than our measurement for Type II Cepheids by $\sim 2\sigma$.

Our mean value of the *p*-factor can be compared to those obtained recently for RR Lyrae and classical Cepheids in Bras et al. (2024) and Trahin et al. (2021) from analysis with the SPIPS code, which are 1.25 ± 0.09 and 1.24 ± 0.14, respectively. The value obtained in this work for BL Her stars is in 1σ agreement with these results; however, it is important to note that we used a different version of the BW method. The dispersion of the *p*-factor for BL Her stars, considering the whole analysed sample, seems to be similar to that of the RR Lyr and classical Cepheids. If we neglect the outlying star VY Pyx, as its uncertainty is much bigger than that of the other stars and mostly statistical, we obtain a much smaller dispersion. The size of our sample is, however, too small to conclusively determine the real intrinsic dispersion of the *p*-factor for BL Her stars.

In Section 2, we mentioned that the selection of the function to model the CCF has quite a significant impact on the obtained values of the *p*-factor. Indeed, *p*-factors of the analysed stars obtained using radial velocities determined from the CCF modelled with the bi-Gaussian and centroid (Nardetto et al. 2017) are systematically lower by ~0.01 (~1%) in the case of the centroid and 0.05 (~5%) for the bi-Gaussian, but the spread of the *p*-factors is identical to when we used the Gaussian. Based on this, we can claim that using a Gaussian to model the CCF is a good approach for BL Her stars as long as it is used consistently for the calibration of the *p*-factor (or *p*-factor − period relation) and the distance determination of the BL Her star, which requires adopting a value for its *p*-factor. In other words, different implementations of the IRSB BW technique might require different *p*-factor values for the same star.

As described in Section 2, we used Lindegren et al. (2021a) corrections for the zero-point offset of parallaxes.

Table 5. Projection factors and radii obtained for the analysed Type II Cepheids.

Name	SBCR	p	$\langle R \rangle$ ($R_\odot$)
VY Pyx	K04a	1.72 ± 0.28	8.50 ± 0.04
	K04b	$\mathbf{1.74 \pm 0.29}$	$\mathbf{8.38 \pm 0.05}$
	S21	1.77 ± 0.29	8.40 ± 0.05
	G21	1.74 ± 0.29	8.41 ± 0.05
BL Her	K04a	1.34 ± 0.09	8.45 ± 0.02
	K04b	$\mathbf{1.34 \pm 0.10}$	$\mathbf{8.27 \pm 0.03}$
	S21	1.36 ± 0.11	8.27 ± 0.03
	G21	1.33 ± 0.10	8.31 ± 0.03
KZ Cen	K04a	1.28 ± 0.08	9.42 ± 0.03
	K04b	$\mathbf{1.35 \pm 0.08}$	$\mathbf{9.25 \pm 0.03}$
	S21	1.42 ± 0.09	9.26 ± 0.03
	G21	1.35 ± 0.08	9.29 ± 0.03
SW Tau	K04a	1.30 ± 0.04	9.38 ± 0.01
	K04b	$\mathbf{1.32 \pm 0.04}$	$\mathbf{9.18 \pm 0.01}$
	S21	1.34 ± 0.05	9.17 ± 0.02
	G21	1.31 ± 0.04	9.23 ± 0.01
V971 Aql	K04a	1.35 ± 0.03	9.73 ± 0.01
	K04b	$\mathbf{1.36 \pm 0.03}$	$\mathbf{9.58 \pm 0.01}$
	S21	1.39 ± 0.03	9.61 ± 0.01
	G21	1.36 ± 0.03	9.62 ± 0.01
V439 Oph	K04a	1.23 ± 0.03	10.98 ± 0.02
	K04b	$\mathbf{1.25 \pm 0.03}$	$\mathbf{10.85 \pm 0.02}$
	S21	1.28 ± 0.03	10.91 ± 0.02
	G21	1.23 ± 0.03	10.87 ± 0.02
RT TrA	K04a	1.31 ± 0.04	10.30 ± 0.02
	K04b	$\mathbf{1.35 \pm 0.05}$	$\mathbf{10.13 \pm 0.03}$
	S21	1.39 ± 0.06	10.16 ± 0.03
	G21	1.35 ± 0.05	10.17 ± 0.03
FM Del	K04a	1.19 ± 0.06	15.28 ± 0.05
	K04b	$\mathbf{1.21 \pm 0.07}$	$\mathbf{15.11 \pm 0.05}$
	S21	1.24 ± 0.08	15.20 ± 0.06
	G21	1.19 ± 0.06	15.12 ± 0.05

Notes. The presented uncertainties are the statistical errors of the BW fit calculated in the Monte-Carlo simulations.

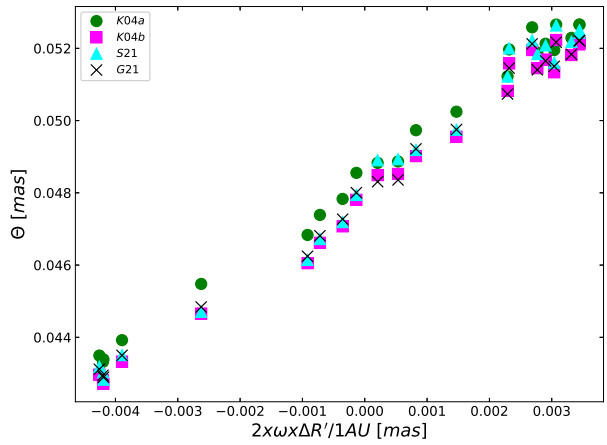

Fig. 5. Relation between the angular diameter inferred from different SBCRs and the integrated radial velocity rescaled using equation (4) for V439 Oph.

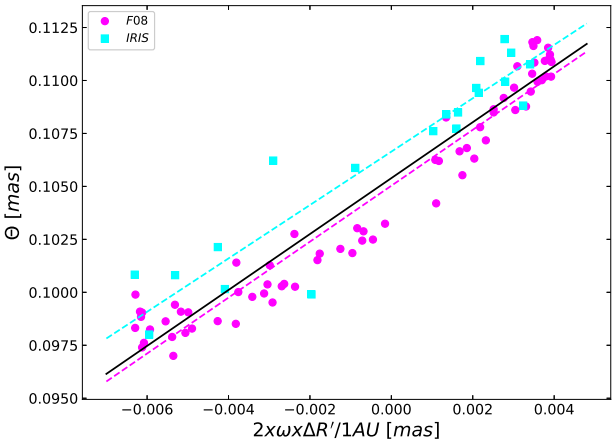

Fig. 6. Baade-Wesselink fit for SW Tau exclusively using IRIS (cyan) and Feast et al. (2008, F08, magenta) K_S band photometry. The black line is the fit using the whole dataset.

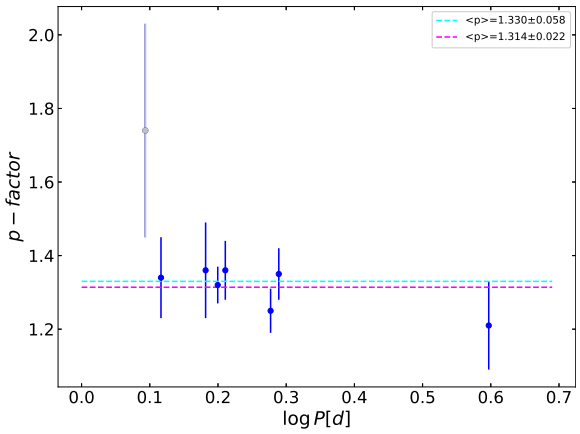

Fig. 7. Period – p-factor relation for BL Her stars. The star marked with a grey point is VY Pyx. The dashed lines denote the weighted mean values of p-factors including VY Pyx (cyan) and without this star (magenta).

However, these corrections are still debated in the literature (e.g. Groenewegen 2021; Molinaro et al. 2023; Cruz Reyes & Anderson 2023), and many authors have suggested that they are overestimated. For comparison, we repeated the BW analysis without introducing any corrections. The resulting values of the p-factors are greater by 0.5–5%, depending on the distance of the star and the size of the zero-point correction, but they agree within the error bars with the values obtained when zero-point corrections are applied. The mean value of the p-factor in this case is greater by 0.03, but the spread is similar in both cases, so if the observed scatter of the p-factor is related to the error on parallaxes, applying corrections from Lindegren et al. (2021b) does not improve the results.

4.2. Radii

The dominating sources of uncertainty on radii are the K_S band light curve systematic uncertainty (~2%) and the parallax, depending on the distance of the star. In the case of VY Pyx, the closest star in our sample, we obtained a total uncertainty of 2% on the measured radius. For FM Del, the most distant star in our sample, the total uncertainty is 7%. The uncertainty related to the V band systematic shift and reddening is negligible, and the uncertainty related to the surface brightness is at a level of 1%.

Table 6. Summary of the errors obtained for p-factors and radii for each star.

Name	$\sigma_{\rm stat}$	$\sigma_{\rm SBCR}$	σ_V	σ_{K_S}	$\sigma_{E(B-V)}$	σ_ω	$\sigma_{\rm total}$	$\sigma_{\rm stat}$	$\sigma_{\rm SBCR}$	σ_V	σ_{K_S}	$\sigma_{E(B-V)}$	σ_ω	$\sigma_{\rm total}$
	p-factors							$\langle R\rangle$ ($R_\odot$)						
VY Pyx	0.29	0.02	0.01	0.03	0.01	0.01	**0.29**	0.05	0.05	0.03	0.11	0.05	0.04	**0.15**
BL Her	0.10	0.01	0.01	0.02	0.01	0.03	**0.11**	0.03	0.09	0.03	0.13	0.05	0.18	**0.25**
KZ Cen	0.08	0.06	0.01	0.02	0.01	0.08	**0.13**	0.03	0.09	0.03	0.15	0.06	0.52	**0.55**
SW Tau	0.04	0.02	0.01	0.02	0.01	0.02	**0.05**	0.03	0.10	0.04	0.15	0.06	0.17	**0.26**
V971 Aql	0.03	0.02	0.01	0.02	0.01	0.07	**0.08**	0.01	0.07	0.03	0.12	0.06	0.48	**0.50**
V439 Oph	0.03	0.02	0.01	0.02	0.01	0.04	**0.06**	0.02	0.06	0.04	0.17	0.07	0.39	**0.44**
RT TrA	0.05	0.03	0.01	0.02	0.01	0.02	**0.07**	0.03	0.07	0.04	0.13	0.06	0.17	**0.24**
FM Del	0.07	0.04	0.01	0.02	0.01	0.08	**0.12**	0.05	0.09	0.04	0.20	0.10	1.04	**1.07**

Notes. The total errors $\sigma_{\rm total}$ are the quadratic sum of the statistical errors of the BW fit $\sigma_{\rm stat}$, errors related to the uncertainty of the surface brightness $\sigma_{\rm SBCR}$, errors related to the systematic shift of the V band light curve σ_V, errors related to the systematic shift of the K_S band light curve σ_{K_S}, errors related to the $E(B-V)$ uncertainty $\sigma_{E(B-V)}$, and errors related to the uncertainty of the parllax σ_ω.

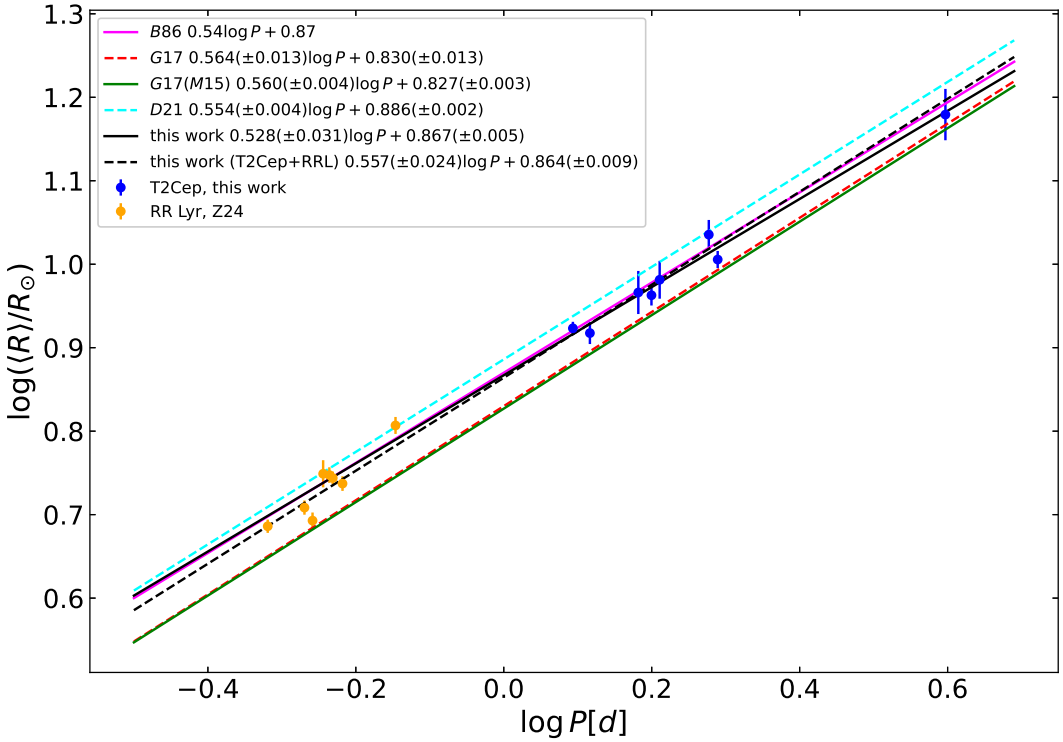

Fig. 8. Period-radius relation for BL Her type stars and the common relation for BL Her and RR Lyr stars based on radii obtained in this work (blue points) and in (Zgirski et al. 2024, orange points). For comparison, we have plotted the relations from the literature: B86 is the empirical relation Burki & Meylan (1986); G17 and G17(M15) are empirical and theoretical relations from Groenewegen & Jurkovic (2017), respectively; and D21 is the theoretical relation from Das et al. (2021).

Radii obtained from the parallaxes without applying Lindegren et al. (2021a) zero-point offset corrections are greater by 0.5–8% (3% on average), depending on the distance of the star and the size of correction but are in agreement within the error bars with values obtained when corrections are applied. The spread of the measurements around the fitted period-radius relation is similar to when we use Lindegren et al. (2021a) corrections.

Figure 8 shows the relation between logarithms of radii and periods of the analysed stars. The errors of the radii in this plot are the total errors from Table 6. As expected, stars with longer periods are bigger, and the relation is linear and quite tight. The line fitted to this relation is

$$\log\langle R\rangle = 0.528(\pm0.031)\log P + 0.867(\pm0.005). \quad (5)$$

We observed in this figure that two stars with very similar periods (namely, V439 Oph and RT TrA) differ quite significantly in radius (about 2σ). It is rather real (not related to any errors), as the bigger star (V439 Oph) has a lower effective temperature (redder colour index what is visible in Figure 2), and thus it is located closer to the red edge of the instability strip.

For comparison, we plotted the period-radius relations from the literature. Burki & Meylan (1986) presented an empirical relation for Type II Cepheids based on radii measured in their BW analysis using optical photometry (which is more sensitive to reddening) and assuming a value of 1.36 for the p-factor, and their relation is in good agreement with our result. Another empirical relation was published by Groenewegen & Jurkovic (2017) based on the temperatures obtained from the spectral energy distribution fitting and luminosities of Type II Cepheids

in the Magellanic Clouds. This relation was derived for short- (BL Her stars) and long-period Type II Cepheids (W Virginis and RV Tau stars), and it predicts radii smaller by ∼8%, but this might be the result of the possibly different mean metallicity of Type II Cepheid populations in the Magellanic Clouds and solar neighbourhood (the latter is almost solar, Wielgórski et al. 2022). The slope of the Groenewegen & Jurkovic (2017) relation is steeper than ours, but it is in agreement within 2σ. We also plotted two theoretical relations. Groenewegen & Jurkovic (2017) published a theoretical relation that is in fact the relation from Marconi et al. (2015) based on the non-linear, convective hydrodynamical models of RR Lyr, which according to Groenewegen & Jurkovic (2017) is relevant for Type II Cepheids. We calculated the zero point of this relation for the solar metallicity. This relation is in a good agreement with the empirical relation from Groenewegen & Jurkovic (2017) and also predicts radii smaller by ∼8% compared to this work. The second theoretical relation is from Das et al. (2021) and was obtained based on non-linear convective models calculated with the `RSP-MESA` code (Smolec & Moskalik 2008; Paxton et al. 2019). They considered different input parameters, and we plotted the relation for the most complex convection parameter set. This relation gives a radii greater by ∼5% compared to our analysis, and the slope is again steeper than that we obtained.

Moreover, we plot in the same figure, the radii of RR Lyr measured with the data collected with identical instruments and analysed with the same BW method by Zgirski et al. (2024). Some authors (e.g. Burki & Meylan 1986; Marconi et al. 2015) have noticed that these two classes of stars can obey single period-radius (and period-luminosity) relations. As can be seen in Figure 8, BL Her and RR Lyr stars can indeed be interpreted as having a common period-radius relation. We fit a common line to BL Her and RR Lyr stars, and our result was

$$\log\langle R\rangle = 0.557(\pm0.024)\log P + 0.864(\pm0.009), \quad (6)$$

with the slope in perfect agreement with (Groenewegen & Jurkovic 2017) empirical and theoretical relations and the (Das et al. 2021) theoretical relation. The exact form of the common relation, including metallicity dependence, requires more measurements of the radii and individual metallicities of both Type II Cepheids and RR Lyr stars.

5. Summary

We used the homogeneous optical and near-infrared photometry and spectra collected within a short span of time and the SBCR variant of the BW method to determine projection factors and radii of eight nearby short-period Type II Cepheids. The obtained values of the p-factors for good quality data (seven stars) are between 1.21 and 1.36, with a typical uncertainty of ∼7%. The mean value amounts to 1.330 ± 0.058 (4% uncertainty). The most significant sources of uncertainty are the dispersion of photometry and radial velocity curves (statistical uncertainty of the final BW fit) and *Gaia* parallaxes. The light and radial velocity curves can be improved by collecting more data, and *Gaia* parallaxes will be more accurate in the future data release. We did not observe any significant dependence of the p-factor on the period of stars.

In the case of radii, the dominant sources of uncertainty are the systematic uncertainty of the K_S band light curve and parallaxes. We derived the period-radius relations for BL Her type stars and the common relation for BL Her and RR Lyr stars (using radii of RR Lyr from Zgirski et al. 2024). The obtained relation for BL Her stars is in good agreement with the previous empirical relation from Burki & Meylan (1986) obtained from BW analysis of Galactic Type II Cepheids. The theoretical relation from (Groenewegen & Jurkovic 2017) predicts radii systematically smaller by ∼8%, while the relation from Das et al. (2021) predicts radii bigger by ∼5%. The common relation for BL Her and RR Lyr stars obtained in this work has a slope that is in very good agreement with theoretical relations.

In the future, we plan to collect data and perform BW analysis of more nearby BL Her type stars as well as of long-period Type II Cepheids (i.e. W Vir type stars). This will allow us to calibrate more precisely both the p-factors and the period-radius relation.

Data availability

Full Tables 1 and 3 are available at the CDS via anonymous ftp to `cdsarc.cds.unistra.fr` (`130.79.128.5`) or via `https://cdsarc.cds.unistra.fr/viz-bin/cat/J/A+A/689/A241`

Acknowledgements. P.W. gratefully acknowledges financial support from the Polish National Science Center grant PRELUDIUM 2018/31/N/ST9/02742. The research leading to these results has received funding from the European Research Council (ERC) under the European Union's Horizon 2020 research and innovation programme (grant agreements No 695099 and No 951549). Support from DIR/2024/WK/02 grant of the Polish Ministry of Science and Higher Education and the Polish National Science Center grants MAESTRO 2017/26/A/ST9/00446 and BEETHOVEN 2018/31/G/ST9/03050 and Polish-French Marie Skłodowska-Curie and Pierre Curie Science Prize awarded by the Foundation for Polish Science is also acknowledged. W.G. and G.P. gratefully acknowledge financial support for this work from the BASAL Centro de Astrofisica y Tecnologias Afines (CATA) AFB-170002. N.N. acknowledges the support of the French Agence Nationale de la Recherche (ANR) under grant ANR-23-CE31-0009-01 (Unlock-pfactor) Based on data collected under the ESO/CAMK PAN - USB agreement at the ESO Paranal Observatory. We thank our colleagues involved in the process of gathering data in OCM. Based on observations collected at the European Organisation for Astronomical Research in the Southern Hemisphere under ESO programmes 099.D-0380(A), 0100.D-0339(B),0100.D-0273(A),0102.D-0281(A), 105.20L8.002, 106.20Z1.001, 106.20Z1.002, 106.21T1.001, 108.22JX.001, 111.24YL.001 and CNTAC programmes CN2016B-150, CN2017A-121, CN2017B-43, CN2018A-40, CN2019B-64, CN2020B-42, CN2020B-69. We are greatly indebted to the staff at the ESO La Silla and Paranal Observatories for excellent support during the many visitor mode runs and for performing the observations in the service mode. This work has made use of data from the European Space Agency (ESA) mission *Gaia* (`https://www.cosmos.esa.int/gaia`), processed by the *Gaia* Data Processing and Analysis Consortium (DPAC, `https://www.cosmos.esa.int/web/gaia/dpac/consortium`). Funding for the DPAC has been provided by national institutions, in particular the institutions participating in the *Gaia* Multilateral Agreement. This publication makes use of data products from the Two Micron All Sky Survey (Skrutskie et al. 2006), which is a joint project of the University of Massachusetts and the Infrared Processing and Analysis Center/California Institute of Technology, funded by the National Aeronautics and Space Administration and the National Science Foundation. This research has made use of the SIMBAD database, operated at CDS, Strasbourg, France (Wenger et al. 2000). We acknowledge with thanks the variable star observations from the AAVSO International Database contributed by observers worldwide and used in this research. Software used in this work: `gaiadr3_zeropoint` (Lindegren et al. 2021a), `Astropy7` (Astropy Collaboration 2013, 2018), `IRAF` (Tody 1986, 1993), `Sextractor` (Bertin & Arnouts 1996), `SCAMP` (Bertin 2006), `SWARP` (Bertin 2010), `DAOPHOT` (Stetson 1987), `NumPy` (van der Walt et al. 2011; Harris et al. 2020), `SciPy` (Virtanen et al. 2020), `Matplotlib` (Hunter 2007). The custom software with GUI used for the Baade-Wesselink IRSB analysis is available on Github: `https://github.com/araucaria-project/balwan.git`.

References

Akima, H. 1970, J. ACM, 17, 589
Anderson, R. I. 2016, MNRAS, 463, 1707
Anderson, R. I., Mérand, A., Kervella, P., et al. 2016, MNRAS, 455, 4231
Astropy Collaboration (Robitaille, T. P., et al.) 2013, A&A, 558, A33
Astropy Collaboration (Price-Whelan, A. M., et al.) 2018, AJ, 156, 123

Baade, W. 1926, Astron. Nachr., 228, 359
Balog, Z., Vinko, J., & Kaszas, G. 1997, AJ, 113, 1833
Balona, L. A. 1977, MNRAS, 178, 231
Barnes, T. G., & Evans, D. S. 1976, MNRAS, 174, 489
Beaton, R. L., Freedman, W. L., Madore, B. F., et al. 2016, ApJ, 832, 210
Becker, W., & Strohmeier, W. 1940, ZA, 19, 249
Benedict, G. F., McArthur, B. E., Feast, M. W., et al. 2011, AJ, 142, 187
Bertin, E. 2006, ASP Conf. Ser., 351, 112
Bertin, E. 2010, Astrophysics Source Code Library [record ascl:1010.068]
Bertin, E., & Arnouts, S. 1996, A&AS, 117, 393
Bhardwaj, A. 2020, JAA, 41, 23
Blanco-Cuaresma, S., Soubiran, C., Heiter, U., & Jofré, P. 2014, A&A, 569, A111
Borgniet, S., Kervella, P., Nardetto, N., et al. 2019, A&A, 631, A37
Brahm, R., Jordán, A., & Espinoza, N. 2017, PASP, 129, 034002
Bras, G., Kervella, P., Trahin, B., et al. 2024, A&A, 684, A126
Breitfelder, J., Kervella, P., Mérand, A., et al. 2015, A&A, 576, A64
Breuval, L., Riess, A. G., Macri, L. M., et al. 2023, ApJ, 951, 118
Burki, G., & Meylan, G. 1986, A&A, 159, 261
Cardelli, J. A., Clayton, G. C., & Mathis, J. S. 1989, ApJ, 345, 245
Challouf, M., Nardetto, N., Mourard, D., et al. 2014, A&A, 570, A104
Coelho, P., Barbuy, B., Meléndez, J., Schiavon, R. P., & Castilho, B. V. 2005, A&A, 443, 735
Cruz Reyes, M., & Anderson, R. I. 2023, A&A, 672, A85
Das, S., Kanbur, S. M., Smolec, R., et al. 2021, MNRAS, 501, 875
Devlen, A., & Acar, M. 2017, AJ, 153, 102
di Benedetto, G. P. 1998, A&A, 339, 858
D'Odorico, S., Cristiani, S., Dekker, H., et al. 2000, SPIE Conf. Ser., 4005, 121
Drimmel, R., & Spergel, D. N. 2001, ApJ, 556, 181
Feast, M. W., Laney, C. D., Kinman, T. D., van Leeuwen, F., & Whitelock, P. A. 2008, MNRAS, 386, 2115
Fouque, P., & Gieren, W. P. 1997, A&A, 320, 799
Gaia Collaboration (Prusti, T., et al.) 2016, A&A, 595, A1
Gaia Collaboration (Brown, A. G. A., et al.) 2021, A&A, 649, A1
Gaia Collaboration (Montegriffo, P., et al.) 2023, A&A, 674, A33
Gallenne, A., Kervella, P., Mérand, A., et al. 2017, A&A, 608, A18
Gieren, W. P., Fouqué, P., & Gómez, M. 1998, ApJ, 496, 17
Gieren, W., Pietrzyński, G., Soszyński, I., et al. 2005, ApJ, 628, 695
Gieren, W., Storm, J., Konorski, P., et al. 2018, A&A, 620, A99
Graczyk, D., Pietrzyński, G., Galan, C., et al. 2021, AA, 649, A109
Groenewegen, M. A. T. 2013, A&A, 550, A70
Groenewegen, M. A. T. 2021, A&A, 654, A20
Groenewegen, M. A. T., & Jurkovic, M. I. 2017, A&A, 603, A70
Harris, C. R., Millman, K. J., van der Walt, S. J., et al. 2020, Nature, 585, 357
Hocdé, V., Nardetto, N., Lagadec, E., et al. 2020, A&A, 633, A47
Hocdé, V., Smolec, R., Moskalik, P., Singh Rathour, R., & Ziółkowska, O. 2024, A&A, 683, A233
Hodapp, K. W., Chini, R., Reipurth, B., et al. 2010, SPIE Conf. Ser., 7735, 77351A
Hunter, J. D. 2007, Comput. Sci. Eng., 9, 90
Jayasinghe, T., Kochanek, C. S., Stanek, K. Z., et al. 2018, MNRAS, 477, 3145
Kaufer, A., & Pasquini, L. 1998, SPIE Conf. Ser., 3355, 844
Kervella, P., Bersier, D., Mourard, D., et al. 2004a, A&A, 428, 587
Kervella, P., Thévenin, F., Di Folco, E., & Ségransan, D. 2004b, A&A, 426, 297
Kervella, P., Mérand, A., & Gallenne, A. 2009, A&A, 498, 425
Koen, C., Marang, F., Kilkenny, D., & Jacobs, C. 2007, MNRAS, 380, 1433
Landolt, A. U. 1992, AJ, 104, 340
Leavitt, H. S. 1908, Ann. Harv. College Obs., 60, 87
Lindegren, L., Bastian, U., Biermann, M., et al. 2021a, A&A, 649, A4
Lindegren, L., Klioner, S. A., Hernández, J., et al. 2021b, A&A, 649, A2
Marconi, M., Coppola, G., Bono, G., et al. 2015, ApJ, 808, 50
Matsunaga, N., Feast, M. W., & Menzies, J. W. 2009, MNRAS, 397, 933
Mérand, A., Kervella, P., Breitfelder, J., et al. 2015, A&A, 584, A80
Molinaro, R., Ripepi, V., Marconi, M., et al. 2023, MNRAS, 520, 4154
Nardetto, N., Stoekl, A., Bersier, D., & Barnes, T. G. 2008, A&A, 489, 1255
Nardetto, N., Fokin, A., Fouqué, P., et al. 2011, A&A, 534, L16
Nardetto, N., Storm, J., Gieren, W., Pietrzyński, G., & Poretti, E. 2014, IAU Symp., 301, 145
Nardetto, N., Poretti, E., Rainer, M., et al. 2017, A&A, 597, A73
Nardetto, N., Gieren, W., Storm, J., et al. 2023, A&A, 671, A14
O'Donnell, J. E. 1994, ApJ, 422, 158
Paxton, B., Smolec, R., Schwab, J., et al. 2019, ApJS, 243, 10
Pepe, F., Mayor, M., Delabre, B., et al. 2000, SPIE Conf. Ser., 4008, 582
Pietrzyński, G., Graczyk, D., Gallenne, A., et al. 2019, Nature, 567, 200
Pilecki, B., Gieren, W., Smolec, R., et al. 2017, ApJ, 842, 110
Pilecki, B., Dervişoğlu, A., Gieren, W., et al. 2018, ApJ, 868, 30
Pojmański, G. 2004, Astron. Nachr., 325, 553
Queloz, D., Mayor, M., Weber, L., et al. 2000, A&A, 354, 99
Ramolla, M., Drass, H., Lemke, R., et al. 2013, Astron. Nachr., 334, 1115
Ramolla, M., Westhues, C., Hackstein, M., et al. 2016, SPIE Conf. Ser., 9911, 99112M
Rastorguev, A. S., & Dambis, A. K. 2011, Astrophys. Bull., 66, 47
Riess, A. G., Casertano, S., Yuan, W., et al. 2021, ApJ, 908, L6
Riess, A. G., Anand, G. S., Yuan, W., et al. 2023, ApJ, 956, L18
Ripepi, V., Molinaro, R., Marconi, M., et al. 2014, MNRAS, 437, 906
Ripepi, V., Cioni, M.-R. L., Moretti, M. I., et al. 2017, MNRAS, 472, 808
Salsi, A., Nardetto, N., Mourard, D., et al. 2021, A&A, 652, A26
Salsi, A., Nardetto, N., Plez, B., & Mourard, D. 2022, A&A, 662, A120
Schlafly, E. F., & Finkbeiner, D. P. 2011, ApJ, 737, 103
Shappee, B., Prieto, J., Stanek, K. Z., et al. 2014, in American Astronomical Society Meeting Abstracts #223, 236.03
Sicignano, T., Ripepi, V., Marconi, M., et al. 2024, A&A, 685, A41
Skrutskie, M. F., Cutri, R. M., Stiening, R., et al. 2006, AJ, 131, 1163
Smolec, R., & Moskalik, P. 2008, Acta Astron., 58, 193
Soszyński, I., Udalski, A., Szymański, M. K., et al. 2008, Acta Astron., 58, 293
Stetson, P. B. 1987, PASP, 99, 191
Storm, J., Gieren, W., Fouqué, P., et al. 2011, A&A, 534, A94
The Araucaria Project (Pietrzyński, G., et al.) 2023, ArXiv e-prints [arXiv:2305.17247]
Thompson, I. B., Kaluzny, J., Pych, W., et al. 2001, AJ, 121, 3089
Tody, D. 1986, SPIE Conf. Ser., 627, 733
Tody, D. 1993, ASP Conf. Ser., 52, 173
Trahin, B., Breuval, L., Kervella, P., et al. 2021, A&A, 656, A102
Udalski, A., Szymanski, M. K., Soszynski, I., & Poleski, R. 2008, Acta Astron., 58, 69
van der Walt, S., Colbert, S. C., & Varoquaux, G. 2011, Comput. Sci. Eng., 13, 22
Virtanen, P., Gommers, R., Oliphant, T. E., et al. 2020, Nat. Meth., 17, 261
Welch, D. L. 1994, AJ, 108, 1421
Wenger, M., Ochsenbein, F., Egret, D., et al. 2000, A&AS, 143, 9
Wesselink, A. J. 1947, Bull. Astron. Inst. Neth., 10, 252
Wielgórski, P., Pietrzyński, G., Pilecki, B., et al. 2022, ApJ, 927, 89
Zgirski, B., Gieren, W., Pietrzyński, G., et al. 2024, A&A, submitted

Appendix A: Figures with the BW analysis

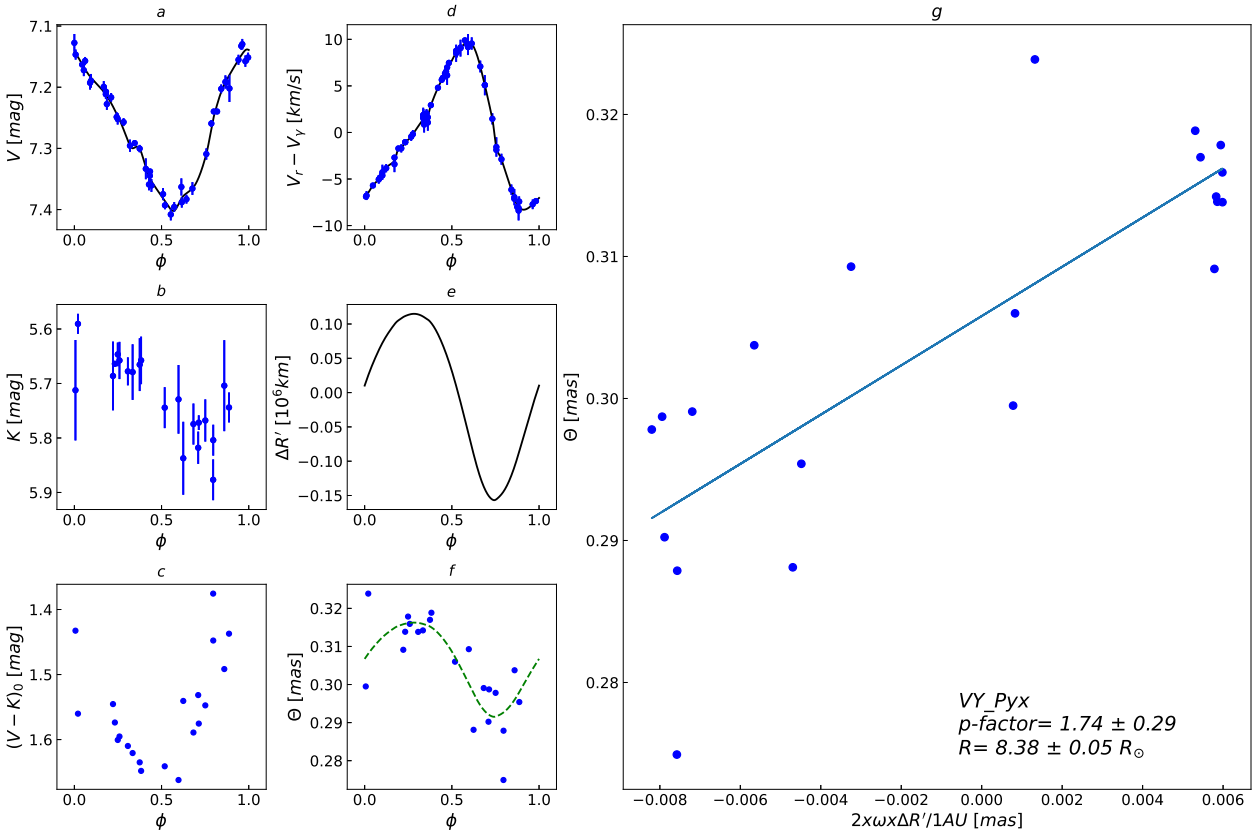

Fig. A.1. Baade-Wesselink analysis of VY Pyx. For a description of the panels, see Figure A.1.

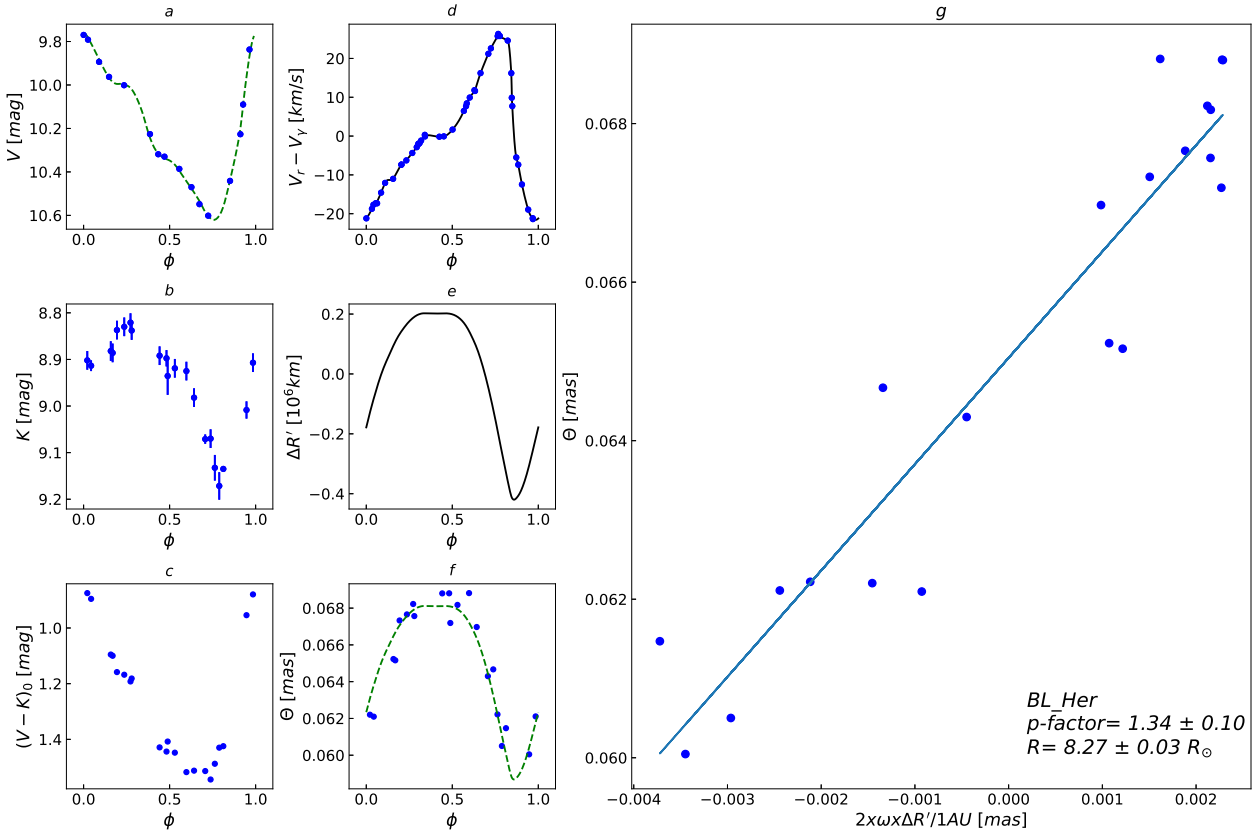

Fig. A.2. Baade-Wesselink analysis of BL Her. For a description of the panels, see Figure A.1.

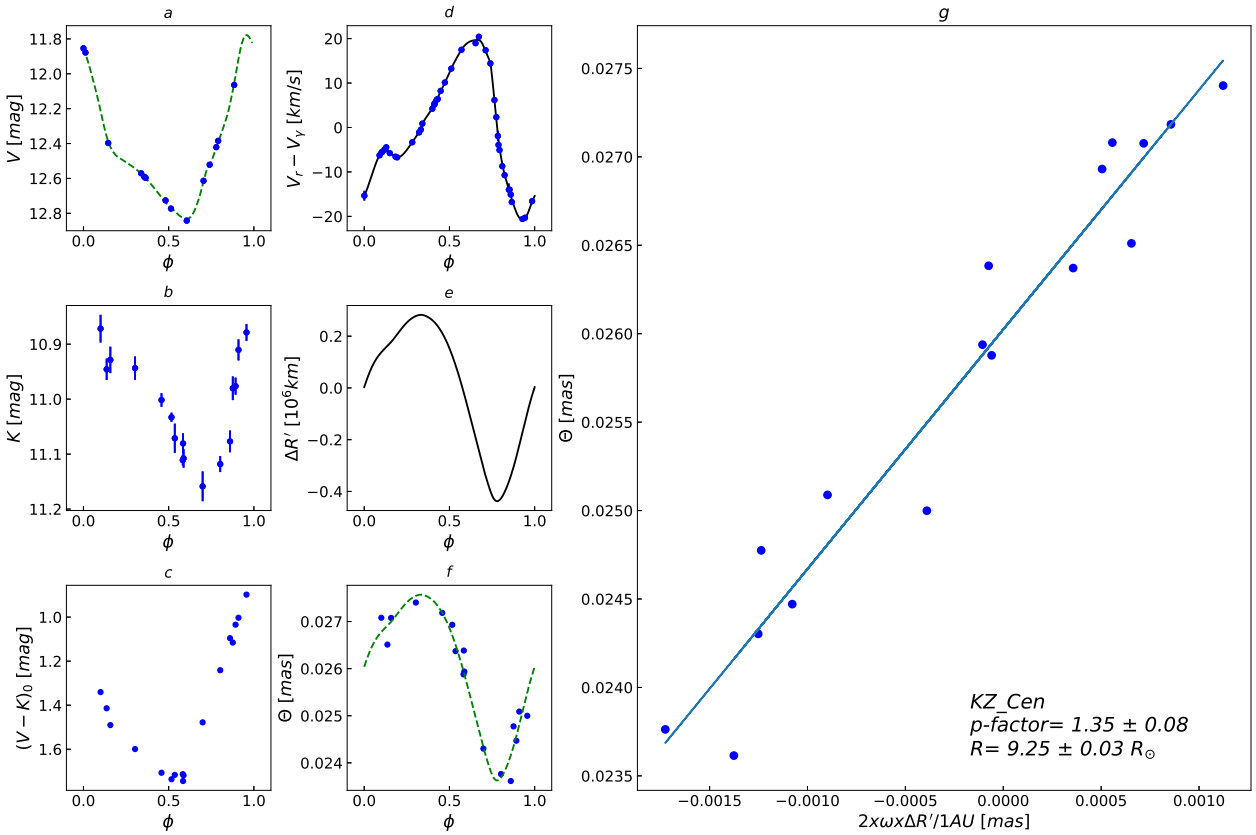

Fig. A.3. Baade-Wesselink analysis of KZ Cen. For a description of the panels, see Figure A.1.

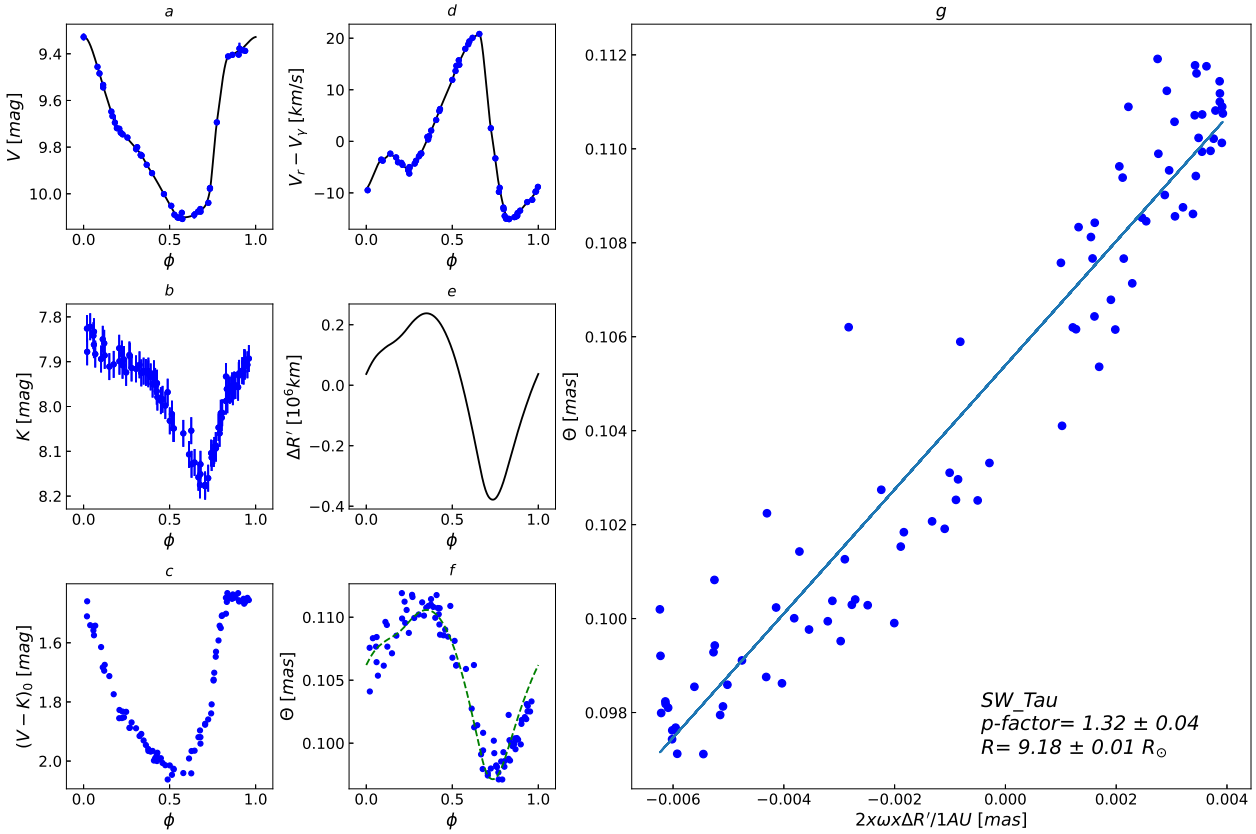

Fig. A.4. Baade-Wesselink analysis of SW Tau. For a description of the panels, see Figure A.1.

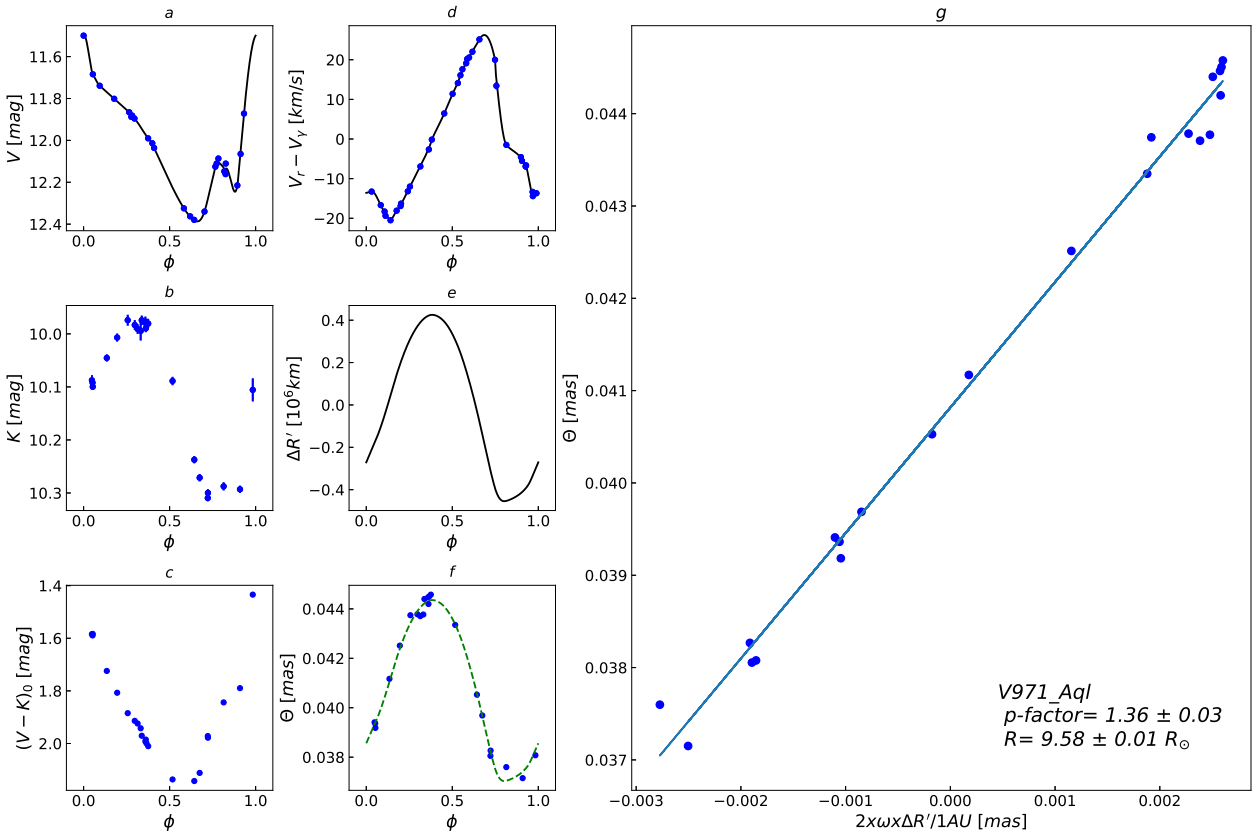

Fig. A.5. Baade-Wesselink analysis of V971 Aql. For a description of the panels, see Figure A.1.

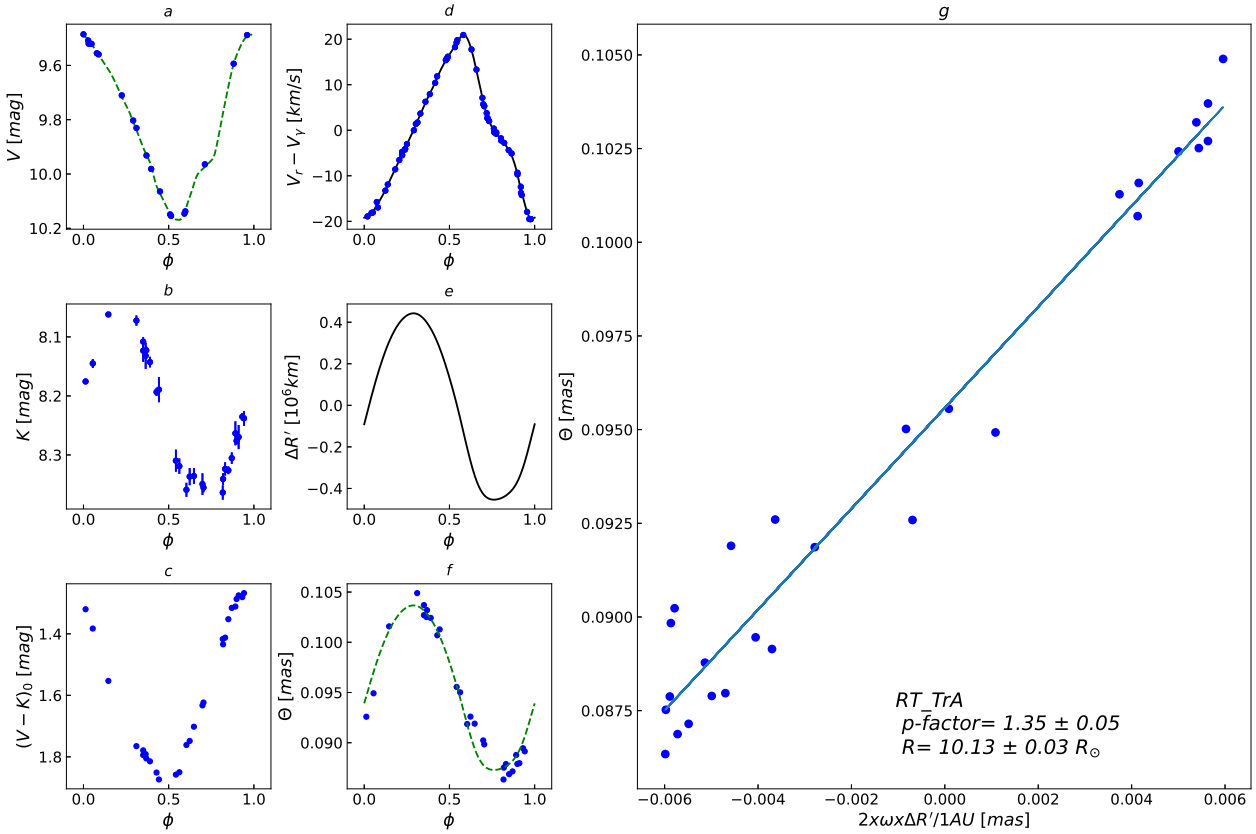

Fig. A.6. Baade-Wesselink analysis of RT TrA. For a description of the panels, see Figure A.1.

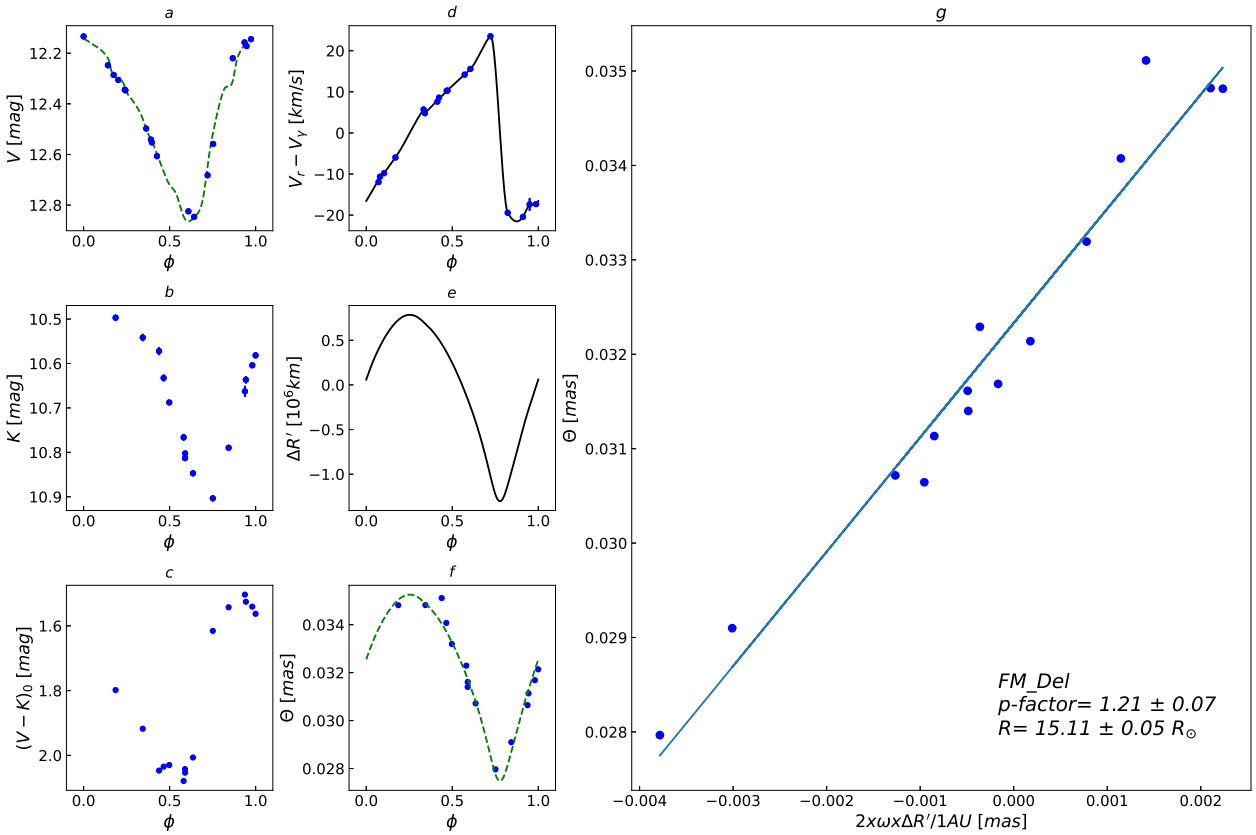

Fig. A.7. Baade-Wesselink analysis of FM Del. For a description of the panels, see Figure A.1.